

VELOCITY FIELD OF COMPRESSIBLE MHD TURBULENCE: WAVELET DECOMPOSITION AND MODE SCALINGS

GRZEGORZ KOWAL

Department of Astronomy, University of Wisconsin, 475 North Charter Street, Madison, WI 53706, USA
Astronomical Observatory, Jagiellonian University, Orla 171, 30-244 Kraków, Poland and
Instituto de Astronomia, Geofísica e Ciências Atmosféricas, Universidade de São Paulo, Rua do Matão 1226, CEP 05508-900, São Paulo, Brazil

AND

ALEX LAZARIAN

Department of Astronomy, University of Wisconsin, 475 North Charter Street, Madison, WI 53706, USA
Draft version October 29, 2018

ABSTRACT

We study compressible MHD turbulence, which holds key to many astrophysical processes, including star formation and cosmic ray propagation. To account for the variations of the magnetic field in the strongly turbulent fluid we use wavelet decomposition of the turbulent velocity field into Alfvén, slow and fast modes, which presents an extension of the Cho & Lazarian (2003) decomposition approach based on Fourier transforms. The wavelets allow to follow the variations of the local direction of magnetic field and therefore improve the quality of the decomposition compared to the Fourier transforms which are done in the mean field reference frame. For each resulting component we calculate spectra and two-point statistics such as longitudinal and transverse structure functions, as well as, higher order intermittency statistics. In addition, we perform the Helmholtz-Hodge decomposition of the velocity field into the incompressible and compressible parts and analyze these components. We find that the turbulence intermittency is different for different components and we show that the intermittency statistics depend on whether the phenomenon was studied in the global reference frame related to the mean magnetic field or it was studied in the frame defined by the local magnetic field. The dependencies of the measures we obtained are different for different components of velocity, for instance, we show that while the Alfvén mode intermittency changes marginally with the Mach number the intermittency of the fast mode is substantially affected by the change.

Subject headings: ISM: structure — MHD — turbulence

1. INTRODUCTION

Astrophysical fluids are magnetized and therefore the astrophysical turbulence is magnetohydrodynamic (MHD) in its nature. Compressible MHD turbulence is a key element for understanding star formation (see Mac Low 2004; Elmegreen & Scalo 2004; McKee & Ostriker 2007, and references therein) and velocity fluctuations determine many of its properties. For instance, in the modern paradigm of star formation that turbulent velocity sweep up the matter from large expands of the interstellar space to create molecular clouds. Thus, it is important to know the statistical properties of the velocity field, e.g. its spectrum that reflects how much energy is associated with the motions at a particular scale (see below).

A further insight into the properties of turbulence, including its generation, consequences and dissipation calls for the use of more sophisticated measures. For example, the processes of magnetic field generation depend on the velocity field vorticity associated with the solenoidal motions, while the processes of compressing gas are determined by the compressible motions. In approaching the problem of decomposing velocity field into solenoidal and dilatational part following the Helmholtz-Hodge decomposition is frequently attempted (see Federrath et al. 2008, 2009). Another approach is the decomposition of the turbulent field in MHD case into basic modes, i.e., Alfvén, slow and fast waves. While this approach is trivial for the case of the strong magnetic field with infinitesimal fluctuations (see Dobrowolny et al. 1980),

Cho & Lazarian (2002, 2003) proposed a *statistical* decomposition of modes in the Fourier space. The statistical nature of the procedure is clear when one considers its application to strongly perturbed magnetic fields. As the Fourier transform is defined in the reference frame related to the mean magnetic field, while the MHD motions happen in respect to the local magnetic field, there is an inevitable contribution of all types of motion to the decomposed modes. However, studying the cases when the real space decomposition was possible in real space, Cho & Lazarian (2003, henceforth CL03) showed that the cross-talk between the modes is small for subAlfvénic turbulence.

Testing of the results in CL03 and increasing the accuracy of the MHD mode decomposition of turbulence is one of the key goals of the present study. In doing so in the present paper we make use of the wavelet transformations in addition to the Fourier transformations. Wavelets (see Meneveau 1991a,b) present a natural way of describing MHD turbulence. Indeed, while in the representation of the Goldreich & Sridhar (1995, henceforth GS95) model of turbulence the anisotropy is frequently described in terms of eddies with parallel k_{\parallel} and perpendicular k_{\perp} wave vectors, the actual description calls for choosing for \parallel and \perp in respect to the *local* magnetic field¹. The latter is really easy to understand, as it is only local magnetic field that influences fluid motions at a given

¹ Due to this fact that closure relations used for the model justification in GS95 are doubtful. The importance of the *local* system of reference was clearly stressed in the works that followed the original GS95 study (Lazarian & Vishniac 1999; Cho & Vishniac 2000; Maron & Goldreich 2001; Cho et al. 2002, 2003; Lithwick & Goldreich 2001; Cho & Lazarian 2002).

point. Wavelets allow for a local description of the magnetized turbulent eddies.

In the paper we decompose the turbulent velocity fields using both wavelets and a more traditional Helmholtz-Hodge decomposition into solenoidal and compressible parts. We feel that the latter decomposition is more justified for the hydrodynamic turbulence than for the MHD turbulence that we study here. However, we feel that the use of the Helmholtz-Hodge decomposition provides an additional, although limited, insight into the properties of compressible motions.

The three major properties of the velocity field that we focus our attention in the paper are turbulence spectra, anisotropies and intermittency. These three measures require further description that we provide below.

While turbulence is an extremely complex chaotic non-linear phenomenon, it allows for a remarkably simple statistical description (see Biskamp 2003). If the injections and sinks of the energy are correctly identified, we can describe turbulence for *arbitrary* Re and Rm . The simplest description of the complex spatial variations of any physical variable, $X(\mathbf{r})$, is related to the amount of change of X between points separated by a chosen displacement \mathbf{l} , averaged over the entire volume of interest. Usually the result is given in terms of the Fourier transform of this average, with the displacement \mathbf{l} being replaced by the wave number \mathbf{k} parallel to \mathbf{l} and $|\mathbf{k}| = 1/|\mathbf{l}|$. For example, for isotropic turbulence the kinetic energy spectrum, $E(k)dk$, characterizes how much energy resides at the interval $k, k+dk$. At some large scale L (i.e., small k), one expects to observe features reflecting energy injection. At small scales, energy dissipation should be seen. Between these two scales we expect to see a self-similar power-law scaling reflecting the process of non-linear energy transfer. We shall attempt to get the power-law scalings for the components of the velocity field.

The presence of a magnetic field makes MHD turbulence anisotropic (Montgomery & Turner 1981; Matthaeus et al. 1983; Shebalin et al. 1983; Higdon 1984; Goldreich & Sridhar 1995)(see Oughton et al. 2003, for review). The relative importance of hydrodynamic and magnetic forces changes with scale, so the anisotropy of MHD turbulence does too. Many astrophysical results, e.g. the dynamics of dust, scattering and acceleration of energetic particles, thermal conduction, can be obtained if the turbulence spectrum and its anisotropy are known (see Lazarian et al. 2009, for review). The knowledge of the anisotropy of Alfvénic mode of MHD turbulence determines the extend of magnetic field wandering influencing heat transfer (Narayan & Medvedev 2001; Lazarian 2006) and magnetic reconnection (Lazarian & Vishniac 1999; Kowal et al. 2009).

We would like to stress that in what follows we discuss the properties of *strong* MHD turbulence. This type of turbulence is not directly related to the amplitude of the magnetic perturbations, however. The low-amplitude turbulence can be strong and isotropically driven turbulence with $\delta B \ll B$ at the injection scale exhibits only a limited range of scales for which it is weak (see Galtier et al. 2000), while at sufficiently small scales it gets strong (see the discussion in Lazarian & Vishniac 1999).

An anisotropic spectrum alone, say $E(\mathbf{k})d\mathbf{k}$, cannot characterize MHD turbulence in all its complexity because it involves only the averaged energy in motions along a particular direction. To have a full statistical description, one needs to know not only the averaged spectrum of a physical vari-

able but higher orders as well. The tendency of fluctuations to become relatively more violent but increasingly sparse in time and space as the scales decreases, so that their influence remains appreciable, is called *intermittency*. The intermittency increases with the ratio of the size scales of injection and dissipation of energy, so the very limited range of scales within numerical simulations may fail to reflect the actual small scale processes. The turbulence intermittency can result in an important intermittent heating of the interstellar medium (Falgarone et al. 2005, 2006, 2007).

In this article we investigate the scaling properties of the structure functions of velocity and its components for compressible MHD turbulence with different sonic and Alfvénic Mach numbers. In §2 we describe the numerical models of compressible MHD turbulence. We decompose velocity into a set of components including the incompressible and compressible parts, and MHD waves: Alfvén, slow and fast using methods described in §3. In §4 we study spectra of velocity and its components. In §5 we study the anisotropy of dissipative structures. We show differences in the structures for different components. In §6 we study the scaling exponents and the intermittency of velocity structures. We show their dependence on the sonic and Alfvén regime of turbulence. In §7 we discuss our results and their relation to the previous studies. In §8 we draw our conclusions.

2. NUMERICAL SIMULATIONS

We used an second-order-accurate essentially nonoscillatory (ENO) scheme (see Cho & Lazarian 2002) to solve the ideal isothermal MHD equations in a periodic box,

$$\frac{\partial \rho}{\partial t} + \nabla \cdot (\rho \mathbf{v}) = 0, \quad (1)$$

$$\frac{\partial \rho \mathbf{v}}{\partial t} + \nabla \cdot \left[\rho \mathbf{v} \mathbf{v} + \left(a^2 \rho + \frac{B^2}{8\pi} \right) \mathbf{I} - \frac{1}{4\pi} \mathbf{B} \mathbf{B} \right] = \mathbf{f}, \quad (2)$$

$$\frac{\partial \mathbf{B}}{\partial t} - \nabla \times (\mathbf{v} \times \mathbf{B}) = 0, \quad (3)$$

where ρ is density, \mathbf{v} is velocity, \mathbf{B} is magnetic field, and a is the isothermal speed of sound. We incorporated the field interpolated constrained transport (CT) scheme (see, e.g., Tóth 2000) into the integration of Eq. (3) to maintain the $\nabla \cdot \mathbf{B} = 0$ constraint numerically. On the right-hand side, the source term \mathbf{f} represents a random solenoidal large-scale driving force. The rms velocity δv is maintained to be approximately unity, so that \mathbf{v} can be viewed as the velocity measured in units of the rms velocity of the system and $\mathbf{B}/(4\pi\rho)^{1/2}$ as the Alfvén velocity in the same units. The time t is in units of the large eddy turnover time ($\sim L/\delta v$) and the length in units of L , the scale of the energy injection. The magnetic field consists of the uniform background field and a fluctuating field: $\mathbf{B} = \mathbf{B}_{\text{ext}} + \mathbf{b}$. Initially $\mathbf{b} = 0$. We use units in which the Alfvén speed $v_A = B_{\text{ext}}/(4\pi\rho)^{1/2} = 1$ and $\rho = 1$ initially. The values of B_{ext} have been chosen to be similar to those observed in the ISM turbulence.

For our calculations, similar to our earlier studies (Kowal et al. 2007), we assumed that $B_{\text{ext}}/(4\pi\rho)^{1/2} \sim \delta B/(4\pi\rho)^{1/2} \sim \delta v$. In this case, the sound speed is the controlling parameter, and basically two regimes can exist: supersonic and subsonic. Note that within our model, supersonic means low β , i.e. the magnetic pressure dominates, and subsonic means high β , i.e. the gas pressure dominates.

TABLE 1
 LIST OF ALL ANALYZED MODELS.

model	B_{ext}	P_{ini}	\mathcal{M}_s	\mathcal{M}_A	res.	max time	max $\delta\rho$	max δV
B1P1	1.0	1.0	0.68 ± 0.03	0.68 ± 0.03	512 ³	7.0	~ 0.3	~ 0.6
B1P.1	1.0	0.1	2.20 ± 0.09	0.69 ± 0.03	512 ³	7.0	~ 0.9	~ 0.7
B1P.01	1.0	0.01	7.0 ± 0.3	0.70 ± 0.04	512 ³	7.0	~ 1.9	~ 0.7
B.1P1	0.1	1.0	0.74 ± 0.06	7.4 ± 0.6	512 ³	7.0	~ 0.2	~ 0.7
B.1P.1	0.1	0.1	2.34 ± 0.08	7.4 ± 0.3	512 ³	7.0	~ 0.8	~ 0.7
B.1P.01	0.1	0.01	7.1 ± 0.3	7.1 ± 0.3	512 ³	7.0	~ 1.5	~ 0.7

We present 3D numerical experiments of compressible MHD turbulence for a broad range of Mach numbers ($0.2 \leq \mathcal{M}_s \leq 7.1$ and $\mathcal{M}_A \sim 0.2$ or ~ 1.8 ; see Table 1). The model name contains two letters: ‘‘P’’ and ‘‘B’’ followed by a number. The letters B and P mean the external magnetic field and the initial gas pressure, respectively, and the numbers designate the value of the corresponding quantity. For example, a name ‘‘B.1P.01’’ points to an experiment with $B_{\text{ext}} = 0.1$ and $P = 0.01$. We understand the Mach number to be defined as the mean value of the ratio of the absolute value of the local velocity v to the local value of the characteristic speed c_s or v_A (for the sonic and Alfvénic Mach number, respectively).

We drove the turbulence at wave scale k equal to about 2.5 (2.5 times smaller than the size of the box). This scale defines the injection scale in our models. We did not set the viscosity and diffusion explicitly in our models. The scale at which the dissipation starts to act is defined by the numerical diffusivity of the scheme. The ENO-type schemes are considered to be relatively low diffusion ones (see, e.g. Liu & Osher 1998; Levy, Puppo & Russo 1999). The numerical diffusion depends not only on the adopted numerical scheme but also on the ‘‘smoothness’’ of the solution, so it changes locally in the system. In addition, it is a time-varying quantity. All these problems make its estimation very difficult and incomparable between different applications. However, the dissipation scales can be estimated approximately from the velocity spectra. In the case of our models we estimated the dissipation scale k_ν at 22 for the resolution 256^3 .

3. DECOMPOSITION OF THE VELOCITY FIELD INTO COMPONENTS

3.1. Compressible and incompressible parts

Using the Hodge generalization of the Helmholtz theorem we can split an arbitrary vector field \mathbf{u} into three components:

$$\mathbf{u} = \mathbf{u}_p + \mathbf{u}_s + \mathbf{u}_l, \quad (4)$$

where each component has specific properties:

- a) Potential component (\mathbf{u}_p) - it is curl-free component, i.e. $\nabla \times \mathbf{u}_p = 0$, so it stems from a scalar potential ϕ :

$$\mathbf{u}_p = \nabla \phi. \quad (5)$$

The scalar potential ϕ is not unique. It is defined up to a constant. This component describes the compressible part of the velocity field.

- b) Solenoidal component (\mathbf{u}_s) - it is divergence-free component, i.e. $\nabla \cdot \mathbf{u}_s = 0$, so it stems from a vector potential Φ :

$$\mathbf{u}_s = \nabla \times \Phi. \quad (6)$$

The vector potential Φ also is not unique. It is defined only up to a gradient field. In the case of velocity this component describes the incompressible part of the field.

- c) Laplace component (\mathbf{u}_l) - it is both divergence-free and curl-free. Laplace component comes from a scalar potential which satisfies the Laplace differential equation $\Delta \phi = 0$.

Thus the decomposition can be rewritten in the form:

$$\mathbf{u} = \nabla \times \Phi + \nabla \phi + \mathbf{u}_l. \quad (7)$$

Applying the divergence operation on both sides and using the divergence-free property of the solenoidal and Laplace components we obtain

$$\nabla \cdot \mathbf{u} = \nabla^2 \phi = \Delta \phi. \quad (8)$$

To find the scalar potential ϕ and the potential field \mathbf{u}_p we have to solve Poisson equation for $\nabla \cdot \mathbf{u}$.

To calculate the vector potential Φ we apply curl operation on both sides of the Eq. (7). Similarly, using the divergence-free property of the potential and Laplace fields we results in equation:

$$\nabla \times \mathbf{u} = \nabla \times \nabla \times \Phi = \Delta \Phi. \quad (9)$$

Here, the calculation of the vector potential Φ requires to solve triple set of Poisson equations, one equation for each component of Φ .

The simulations with periodic boundary conditions have the advantage, that we can solve the Poisson equation using Fourier methods. The Fourier components of the velocity field are transformed back to the real space then, and further analyzed.

3.2. Separation into the Alfvén, Slow and Fast modes

Another very important type of decomposition is the separation of velocity into the MHD waves: Alfvén, slow and fast. In this paper, we use an extended mode based on a technique described in CL03. The procedure of decomposition is performed in the Fourier space by a simple projection of the velocity Fourier components $\hat{\mathbf{u}}$ on the direction of the displacement vector for each mode (see 1). The directions of the displacement vectors $\hat{\xi}_s$, $\hat{\xi}_f$, and $\hat{\xi}_A$ corresponding to the slow mode, fast and Alfvén modes, respectively, are defined by their unit vectors

$$\hat{\xi}_s \propto (-1 + \alpha - \sqrt{D})k_{\parallel} \hat{\mathbf{k}}_{\parallel} + (1 + \alpha - \sqrt{D})k_{\perp} \hat{\mathbf{k}}_{\perp}, \quad (10)$$

$$\hat{\xi}_f \propto (-1 + \alpha + \sqrt{D})k_{\parallel} \hat{\mathbf{k}}_{\parallel} + (1 + \alpha + \sqrt{D})k_{\perp} \hat{\mathbf{k}}_{\perp}, \quad (11)$$

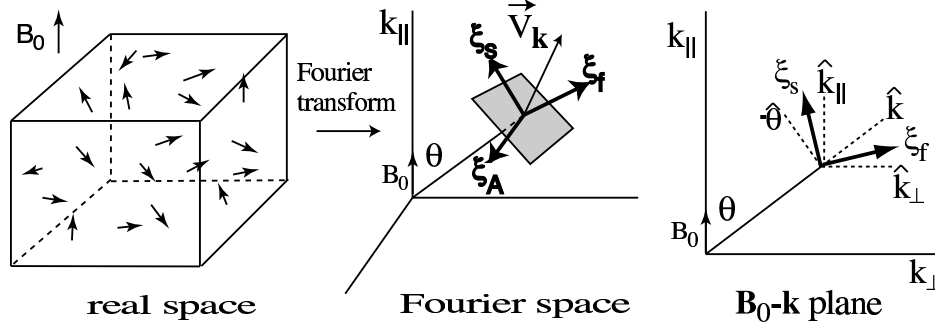


FIG. 1.— Graphical representation of the mode separation method. We separate the Alfvén, slow and fast modes by the projection of the velocity Fourier component \mathbf{v}_k on the bases $\hat{\xi}_A$, $\hat{\xi}_s$ and $\hat{\xi}_f$, respectively. Figure taken from CL03

$$\hat{\xi}_A = -\hat{\varphi} = \hat{\mathbf{k}}_{\perp} \times \hat{\mathbf{k}}_{\parallel}, \quad (12)$$

where \mathbf{k}_{\parallel} and \mathbf{k}_{\perp} are the parallel and perpendicular to \mathbf{B}_{ext} components of wave vector, respectively, $D = (1 + \alpha)^2 - 4\alpha \cos^2 \theta$, $\alpha = a^2/V_A^2$, θ is the angle between \mathbf{k} and \mathbf{B}_{ext} , and $\hat{\varphi}$ is the azimuthal basis in the spherical polar coordinate system. The Fourier components of each mode can be directly used to calculate spectra. For other measures, such as structure functions, we transform them back to the real space.

We extend the CL03 technique by introducing an additional step before the Fourier separation, in which we decompose each component of the velocity field into orthogonal wavelets using discrete wavelet transform (see Antoine 1999, e.g.)

$$\mathbf{U}(a, \mathbf{w}_{lmn}) = a^{-N/2} \sum_{\mathbf{x}_{ijk}} \psi \left(\frac{\mathbf{x}_{ijk} - \mathbf{w}_{lmn}}{a} \right) \mathbf{u}(\mathbf{x}_{ijk}) \Delta^N \mathbf{x}, \quad (13)$$

where \mathbf{x}_{ijk} and \mathbf{w}_{lmn} are N -dimensional position and translation vectors, respectively, a is the scaling parameter, $\mathbf{u}(\mathbf{x}_{ijk})$ is the velocity vector field in the real space, $\mathbf{U}(\mathbf{x}_{ijk})$ is the velocity vector field in the wavelet space, and ψ is the orthogonal analysing function called wavelet. The sum in the equation is taken over all position indices. We use 12-tap Daubechies wavelet as an analyzing function and fast discrete version of the wavelet transform (Antoine 1999), thus, as a result we obtain a finite number of wavelet coefficients. After the wavelet transform of the velocity we calculate the Fourier representation of each wavelet coefficient and perform its individual separation into the MHD waves in the Fourier space using the CL03 method and then update the Fourier coefficients of all MHD waves iterating over all wavelets. In this way we obtain a Fourier representation of the Alfvén, slow and fast waves. The final step is the inverse Fourier transform all all wave components.

This additional step allows for important extension of the CL03 method, namely, allows for the local definition of the mean magnetic field and density used to calculate α and D coefficients. Since the individual wavelets are defined locally both in the real and Fourier spaces, the averaging of the mean field and density is done only within the space of each wavelet.

We can summarize the extended version of the MHD waves decomposition into the following steps:

1. Perform wavelet transform of all velocity components.
2. Iterate over all wavelet coefficients.
 - (a) Calculate Fourier representation of the current wavelet.

- (b) Calculate the mean density and magnetic field within the space occupied by the wavelet.
- (c) Perform the CL03 separation in the Fourier space.
- (d) Add the contribution from the separated wavelet to the Fourier representation of the Alfvén, slow and fast modes.

3. Perform the inverse Fourier transform of the Alfvén, slow and fast wave components.

4. SPECTRA OF THE VELOCITY COMPONENTS

In order to obtain one-dimensional (1D) spectra we first calculate Fourier transform of a quantity and next multiply it by its conjugation. We can use this procedure because we used a fully periodic domain. The 3D spectra must be averaged or integrated over shells $k_n \leq k < k_{n+1}$. We used a simple integration by summing all squared amplitudes at given shell. For each model we have collected data several time steps. We used them to increase the size of sample and to measure the time departures of the spectra from their mean profiles. We should note here, however, that the time averaging and standard deviations were calculated in log-log space. Otherwise, we could result in taking logarithm of negative number, e.g. for ranges of k where the power spectrum has very small values (of order 10^{-6} or less).

In Figure 2 we present spectra for velocity field (top row) and its incompressible and compressible parts (middle and bottom rows, respectively) for models with different sonic Mach numbers. The left column in Figure 2 shows models with a strong magnetic field ($\mathcal{M}_A \sim 0.5 - 0.7$), while the right column shows the corresponding models but with a weak magnetic field ($\mathcal{M}_A \sim 1.7 - 1.9$). The spectra are averaged over several time snapshots taken for a fully developed turbulence. This allowed us to estimate the spectra time variance which is shown as the gray area plotted around the mean profiles. We see that in all cases those variances are small.

Within the inertial range, which we estimated to be $k \in [4, 20]$, the spectra of velocity field slightly change their spectral indices with the value of \mathcal{M}_s . In the case of subAlfvénic models the spectral index is close to $-5/3$. In the case of superAlfvénic turbulence, the indices do not change with \mathcal{M}_s as well, and all models show the same, close to -2 , value of the spectral index at low wave numbers, which is reflection of the presence of shocks in the system. Proceeding toward smaller scales we observe a bump with spectral index approaching $-5/3$ which could be explained by the growing importance of the mean field at these scales and dominance of Alfvén wave. The velocity fluctuations have comparable amplitudes for corresponding scales for all models. It means, that the strength of

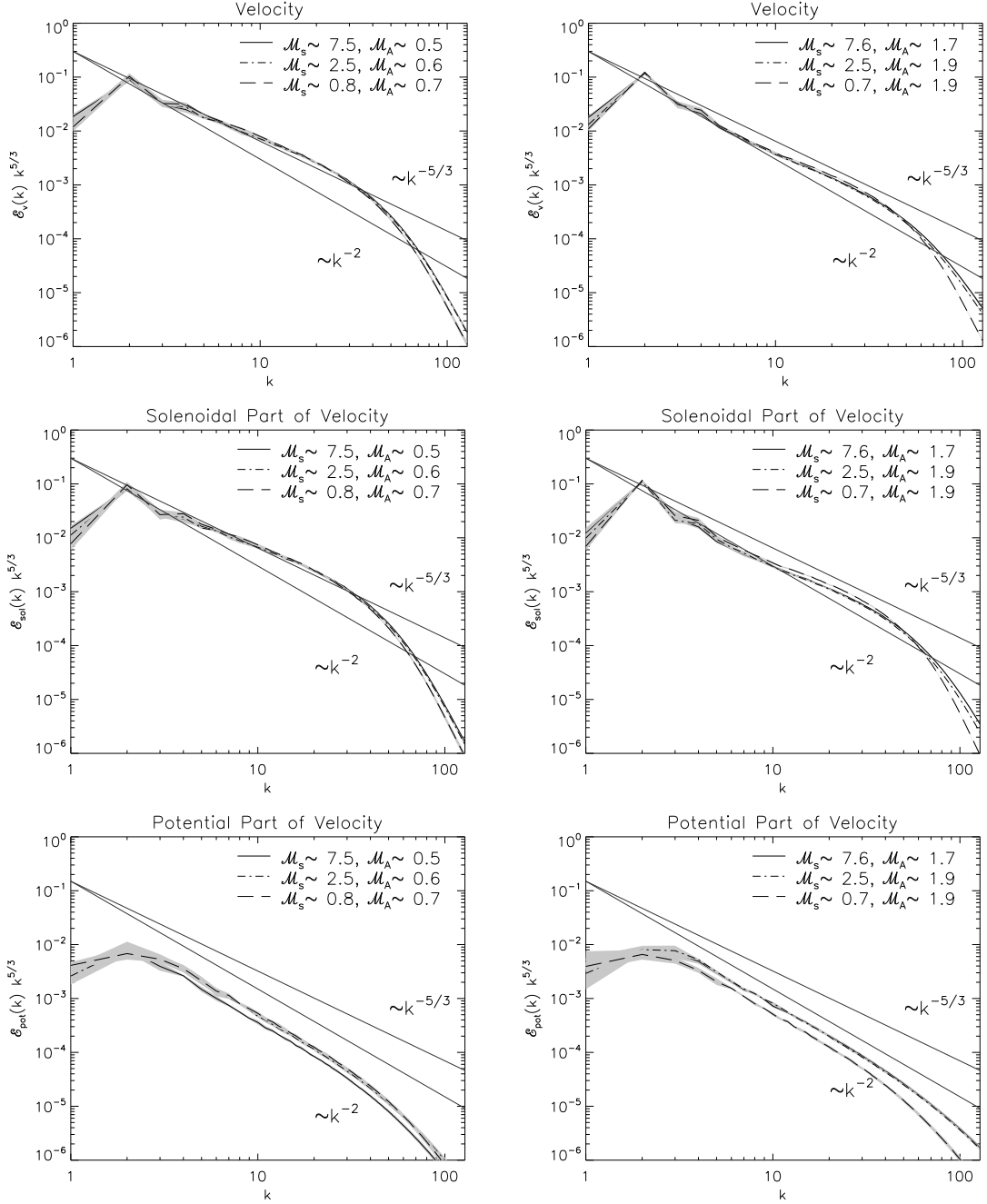


FIG. 2.— Spectra of the velocity field (top row) and its solenoidal and potential parts (middle and bottom rows, respectively) for experiments with different sonic Mach numbers for two magnetic regimes: subAlfvénic (left column) and superAlfvénic (right column). The gray area denotes the degree of time variance of the spectra.

fluctuations at particular scale k within the inertial range does not depend on M_s .

The total velocity field contains two components: solenoidal, which is equivalent to the incompressible part, and potential, which contains the compressible part of the field and the remaining part which is curl- and divergence-free. In Table 2 we show the percentage contribution of each component to the total velocity field. We see, that the compressible part constitutes only a fraction of the total field. However, the magnitude of this fraction is different for sub- and supersonic models. In the case of subAlfvénic turbulence it is about 3% in subsonic models and about 7% in supersonic models,

which confirms a higher efficiency of the compression in the presence of supersonic flows. Furthermore, the fraction also changes when we compare models with strong and weak magnetic fields. The velocity field, in the presence of a weak magnetic field, contains about 5% of the compressible part in the model with $M_s \sim 0.7$ and even up to 16% in models with $M_s > 1$. The consequence of the presence of a strong magnetic field results in a reduction of the compressible part of the velocity field by a factor 2. This indicates a substantial role of the magnetic field in the damping of the generation of the compressible flows.

Due to a substantial dominance of the incompressible part

TABLE 2
PERCENTAGE AMOUNT OF THE KINETIC ENERGY CONTAINED WITHIN EACH VELOCITY COMPONENT. ERRORS CORRESPOND TO A MEASURE OF THE TIME VARIATION.

\mathcal{M}_s	\mathcal{M}_A	$V_{\text{incomp.}}$	$V_{\text{comp.}}$	V_A	V_s	V_f
~ 0.7	~ 0.7	$96.5^{\pm 0.8}$	$3.3^{\pm 0.8}$	$58^{\pm 4}$	$37^{\pm 3}$	$4.8^{\pm 0.7}$
~ 2.2	~ 0.7	$93^{\pm 2}$	$7^{\pm 2}$	$58^{\pm 5}$	$33^{\pm 4}$	$9^{\pm 2}$
~ 7.0	~ 0.7	$92^{\pm 2}$	$7^{\pm 2}$	$56^{\pm 4}$	$36^{\pm 4}$	$8.0^{\pm 0.7}$
~ 0.7	~ 7.4	$95^{\pm 2}$	$5^{\pm 2}$	$52^{\pm 4}$	$42^{\pm 4}$	$6.2^{\pm 0.8}$
~ 2.3	~ 7.4	$86^{\pm 1}$	$14^{\pm 2}$	$47^{\pm 3}$	$37^{\pm 4}$	$16^{\pm 2}$
~ 7.1	~ 7.1	$84^{\pm 2}$	$16^{\pm 2}$	$47^{\pm 4}$	$33^{\pm 4}$	$20^{\pm 2}$

of the velocity field, we expect that its spectra should follow the spectra for the total velocity field. In the middle row of Figure 2 we present the spectra for the incompressible part of the velocity field. We see that the spectra, at least within the inertial range, are very similar to those observed for the velocity field. Also the spectral indices have very close values for models with strong and weak magnetic field.

In the case of compressible turbulence, more interesting are spectra of the potential component (the bottom row in Figure 2). We see that these spectra are different from those for the incompressible part. The strength of the compressible part confirms the change of contribution of the compressible part. It is smaller for subsonic models than for supersonic models, which can be seen in the bottom row of Figure 2. However, both supersonic models have almost the same spectra with the spectral indices about -2 for subAlfvénic turbulence and for superalfvénic turbulence. Both supersonic spectra show almost exactly the same profiles and amplitudes at all scales, even within the dissipation range. This means that the amount of compressible part of the velocity field do not change with \mathcal{M}_s when its value is larger than one.

The second decomposition, more important for MHD turbulence, separates the velocity field into three different MHD waves: an incompressible Alfvén and slow and fast magneto acoustic waves, which both are compressible. In Table 2 we included the percentage amount of these components in the total velocity field. As we see, the most of energy is contained in the Alfvén wave. It is almost 60% in the case of subAlfvénic turbulence, and about 50% for superAlfvénic turbulence. The slow wave contains approximately 1/3 of the total energy. However, for superAlfvénic case, this amount is slightly higher. Table 2 suggests, that the slow wave is weaker when the turbulence become supersonic. We do not see similar behavior for the Alfvén wave in the case of models with a strong magnetic field. This effect could take place also in the superAlfvénic models, but it is weakened by relatively large errors. An interesting dependence is observed in the case of the fast wave. Although, the fast wave is the weakest among all MHD waves, it strongly depends on the regime of turbulence. Similarly to the compressible part of velocity field, it is stronger for models with weak magnetic field. In addition, it is much stronger when turbulence are supersonic, but this strength seems to be weakly dependent on the sonic Mach number.

In Figure 3 we present spectra for the MHD waves for all models from Table 1. In the left column we show spectra for models with a strong magnetic field, while in the right column spectra for models with a weak magnetic field. Top, middle and bottom rows show the Alfvén, slow and fast mode

spectra, respectively. In the case of Alfvén wave we see that the spectral indices depend on the sonic Mach number weakly. All indices lay between -2 and $-5/3$ with a slight dependence on \mathcal{M}_s . This is similar situation like for spectra of velocity field. For superAlfvénic models we observe similar situation, however, since the mean field is weaker, the power spectra are shifted down to smaller amplitudes. The similarities in spectra between the Alfvén mode and velocity field are due to the fact, that the Alfvén mode constitutes the major part of the velocity field.

The slow wave, however, constitutes also a substantial part of the velocity field. Looking closer in the spectral indices for the slow mode plotted in Figure 3 we see that their values do not change significantly with \mathcal{M}_s when mean magnetic field is strong, although it is difficult to determine one spectral index do to changing profile of the spectrum with the wave number. There seems to be stronger dependence of the spectral indices on the sonic Mach number when the mean field is weak, where the inertial region is easier to determine.

The fast wave, the weakest mode of the velocity field, shows two types of spectra depending on the sonic and Alfvénic regime of turbulence. In the case of subsonic models we see that the fast mode spectrum has index close to -2 . When the field is weak, the value of index is a bit flatter then -2 . This indicates a clear dissimilarity of spectra for subsonic turbulence, for different strength of the magnetic field. In supersonic models, however, the spectral indices are going closer to the value -2 , independently of the sonic Mach number. This signifies a growing role of the shock compression in supersonic turbulence.

5. ANISOTROPY

If we want to study the anisotropy of turbulent structures we need to introduce a reference frame. In the case of magnetized turbulence the reference frame is defined in the natural way by the local mean magnetic field. The local magnetic field is computed using the procedure of smoothing by a three-dimensional Gaussian profile with the width equal to the separation length. Since the volume of smoothing grows with the separation length l , the direction of local mean magnetic field might change with l at arbitrary point. This is an extension of procedures employed in Cho & Vishniac (2000) and Cho et al. (2002).

To analyze the anisotropy of different components of the velocity field we use the total structure function

$$S^{(p)}(l) = \langle \delta v(\mathbf{l})^p \rangle, \quad (14)$$

where δv is a total increment

$$\delta v(\mathbf{l}) = |\mathbf{v}(\mathbf{x} + \mathbf{l}) - \mathbf{v}(\mathbf{x})|, \quad (15)$$

and $\langle \dots \rangle$ denotes an ensemble averaging. For each component we evaluate the parallel and perpendicular structure functions taking respectively the directions of the separation length \mathbf{l} parallel and perpendicular to the local mean magnetic field. To show the degree of anisotropy we plot the structure function in direction perpendicular to the local mean magnetic field as a function of the parallel structure function for corresponding separation lengths. In this way we show also, how the anisotropy changes with the scale of structures.

In Figure 4 we present the degree of anisotropy for the velocity field (top row) and for the solenoidal (incompressible) and potential (compressible) parts of the velocity fields (middle and bottom row, respectively). The left and right columns

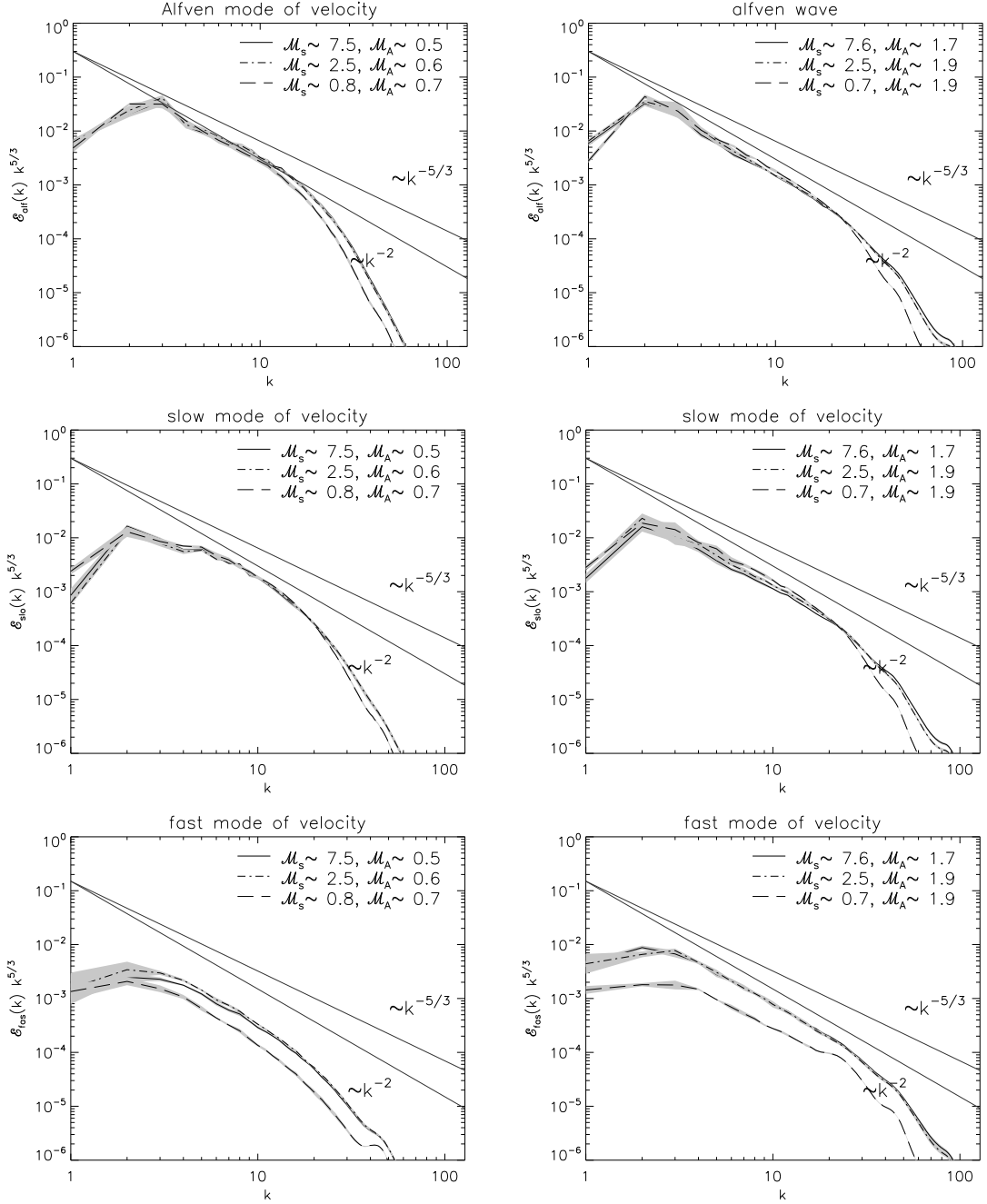


FIG. 3.— Spectra of the Alfvén, slow and fast mode (top, middle and bottom rows, respectively) of the velocity field for experiments with different sonic Mach numbers in two regimes: subAlfvénic (left column) and superAlfvénic (right column). The gray area denotes the degree of departures at single time snapshots from the mean profile.

correspond to the sub- and superAlfvénic turbulence, respectively. The gray areas under points show the degree of time variances of the structure functions used to plot anisotropies. In each plot of Figure 4 we also plot lines corresponding to the isotropic structure, $l_{\parallel} \sim l_{\perp}$, and theoretical, $l_{\parallel} \sim l_{\perp}^{2/3}$ (Goldreich & Sidhar 1995, GS95). We see that the structures of velocity and its incompressible part show the GS95 type anisotropy, for both Alfvénic regimes. Another conclusion coming from these plots is that the anisotropy is insensitive on the value of the sonic Mach number. All curves have the same shape in the presented plots. The one noticeable difference is that in the case of subAlfvénic turbulence the anisotropy

slightly changes with the values of S_2^{\parallel} , which are related to the scale of structures. Lower values of S_2^{\parallel} correspond to the small-scale structures, larger to the large-scale structures. In this description we can suspect, that the small scale structures are almost isotropic. The degree of anisotropy grows with the scale, and for the large scale structures it exceeds somewhat the GS95 anisotropy. In the case of a weak external magnetic field the degree of anisotropy is uniform over the whole range of scales, but also here we notice very good agreement with GS95 anisotropy. The compressible component of the velocity field behaves differently. For subAlfvénic turbulence it is almost perfectly isotropic and independent of the sonic Mach

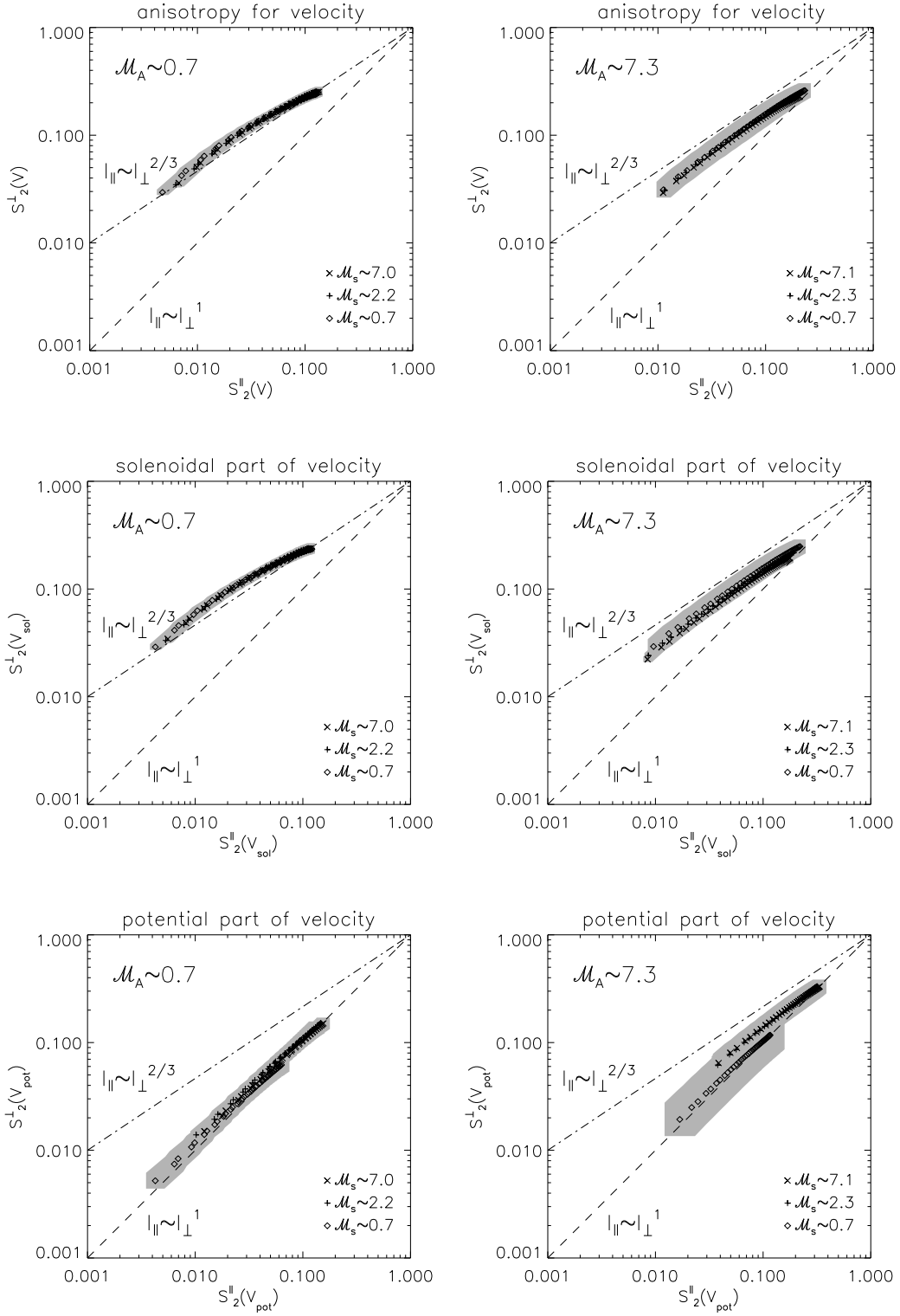


FIG. 4.— Anisotropy of the structures of the velocity (top row) and solenoidal and potential parts of the velocity (middle and bottom rows, respectively). The left column shows anisotropies for subAlfvénic models, the right column plots are for superAlfvénic models. To show anisotropy we use the 2nd-order total structure functions, parallel and perpendicular to the local mean magnetic field. Points corresponds to the mean profiles of the structure functions averaged over several snapshots. The gray areas under points correspond to the degree of departures of the structure functions in time.

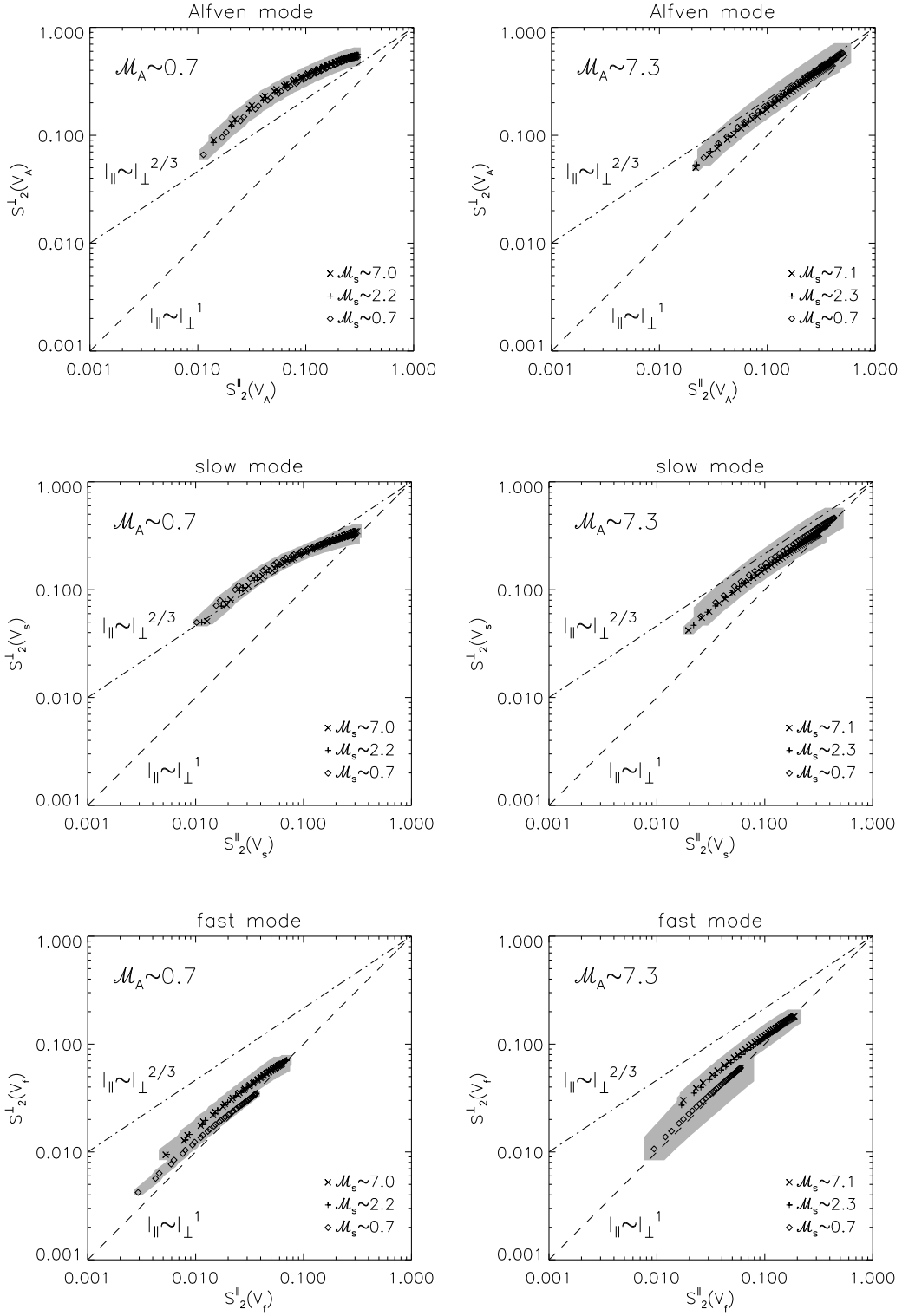


FIG. 5.— Anisotropy of the structures of the Alfvén, slow and fast modes (top, middle and bottom rows, respectively). To show the anisotropy we use the 2nd-order total structure functions, parallel and perpendicular to the local mean magnetic field. Points correspond to the mean profiles of the structure functions averaged over several snapshots. The gray areas under points correspond to the degree of departures of the structure functions in time.

number. In the superAlfvénic turbulence, however, we see, that structure of subsonic potential field is isotropic on average, although there are relatively large time departures from the isotropy. On contrary, in the case of supersonic turbulence, the structure of the potential field contains a higher amount of anisotropic structures and the degree of anisotropy aims to the GS95-law.

In Figure 5 we show the anisotropy of structures for Alfvén, slow and fast modes of velocity. The separation of the modes is performed with the respect of the local mean magnetic field. The first comparison of these plots shows, that the degree of anisotropy does not depend on the sonic Mach number for the Alfvén and slow modes. The anisotropy of fast mode, similarly to the case of the compressible part of the velocity, depends on the regime of sonic motions. If the fluid motions are subsonic the structures of the fast waves is more isotropic. When the fluid motions are supersonic, more structures become anisotropic. We should note here, that speaking about the anisotropy of structures we understand a mean anisotropy of all structures of the analyzed field. Individual structures in the turbulence evolve and yield at different deformations resulting in a constant change of the degree of the anisotropy. In this situation, speaking about an anisotropy, we are relating to the mean dominant anisotropy of all structures in the system.

The two remaining modes, the Alfvén and slow, show very similar anisotropies to those observed in velocity and its incompressible part. We see that basically the degree of anisotropy of structures in these two modes is closer to GS95. In addition, the presence of a strong magnetic field results in a much stronger bending of the curves in right plots of Figure 5 signifying changes of the anisotropy with the scale of the structure. The curves in plots for superAlfvénic models are almost straight and independent of the values of S_2^{\parallel} .

6. SCALING EXPONENTS AND INTERMITTENCY

Intermittency is an essential property of astrophysical fluids. As intermittency violates self-similarity of motions, it is impossible to naively extrapolate the properties of fluids obtained computationally with a relatively low resolution to the actual astrophysical situations. In astrophysics the intermittency affects turbulent heating, momentum transfer, interaction with cosmic rays, radio waves and many more essential processes. Physical interpretation of intermittency started after the work by Kolmogorov, but the first successful model was presented by She & Lévéque (1994). The scaling relations suggested by She & Lévéque (1994) relate $\zeta(p)$ to the scaling of the velocity $v_l \sim l^{1/g}$, the energy cascade rate $\epsilon_l^{-1} \sim l^{-x}$, and the co-dimension of the dissipative structures C :

$$\zeta(p) = \frac{p}{g}(1-x) + C \left(1 - (1-x/C)^{p/g}\right). \quad (16)$$

Parameter C is related to the dimension of the dissipative structures D through relation $C = 3 - D$ (Müller & Biskamp 2000). In hydrodynamical turbulence, according to the Kolmogorov scaling, we have $g = 3$ and $x = 2/3$. Vortex filaments, which are one-dimensional structures, correspond to $C = 2$ ($D = 1$). In the MHD turbulence we also observe current sheets, which are two-dimensional dissipative structures and correspond to $C = 1$ ($D = 2$). For these two types of dissipative structures we obtain two different scaling relations (substituting $g = 3$ and $x = 2/3$):

$$\zeta(p) = \frac{p}{9} + 2 \left[1 - (2/3)^{p/3}\right] \text{ for } C = 2 \quad (17)$$

and

$$\zeta(p) = \frac{p}{9} + 1 - (1/3)^{p/3} \text{ for } C = 1. \quad (18)$$

Relation (17) is often called the She & Lévéque scaling (She & Lévéque 1994), while relation (18), the Müller-Biskamp scaling (Müller & Biskamp 2000). There are theoretical arguments against the model (see Novikov 1994), but so far the She & Lévéque scaling is the best for reproducing the intermittency of incompressible hydrodynamic turbulence.

Structure functions can be calculated with respect to the global or local reference frames. By the scaling exponents calculated in the global reference frame we understand the scaling exponents calculated from the structure functions averaged over all directions. In the local reference we distinguish between directions parallel and perpendicular to the local mean magnetic field. In this way we define the reference frame locally by the direction of the local magnetic field.

In Figures 6 and 7 we show scaling exponents for the velocity and all its parts and waves calculated in the global reference frame. In the top left plot of Figure 6 we see that for the subAlfvénic turbulence the scaling exponents of velocity follow the She-Lévéque (S-L) scaling with $D = 1$. Supported by the theoretical considerations we can say that most of the dissipative structures are one-dimensional. Even though the scalings are not perfectly independent of the value of \mathcal{M}_s , since we see somewhat lower values of ζ for higher p , the differences between these values for models with different sonic Mach numbers are within their error bars, thus it is relatively difficult to state that the scalings are completely independent or only weakly dependent of the values of \mathcal{M}_s . Looking in the corresponding plot for models with a weak magnetic field we clearly see that the spread of curves for different sonic Mach numbers is much higher than in the previous case. For subsonic model the scaling exponents of velocity follow very well the theoretical curve defined by the S-L scaling with parameter D corresponding to one-dimensional structures. The model with $\mathcal{M}_s \sim 2.3$, however, follows perfectly the S-L scaling with $D = 2$ corresponding to the two-dimensional dissipative structures. Moreover, models with even higher values of the sonic Mach number have the scaling exponents for $p > 3$ somewhat below the S-L scaling with $D = 2$. These observations suggest that the scaling exponents of the velocity change with the sonic Mach number but only in the case of weak magnetic field turbulence. The presence of a strong magnetic field significantly reduces these changes and preserves the generation of the dissipative structures of higher than one dimensions.

After the decomposition of velocity into its incompressible and compressible parts we also calculate their scaling exponents. In the middle and right columns of Figure 6 we show the incompressible and compressible parts of the velocity field, respectively. The incompressible part is strong. It constitutes most of the velocity field thus it is not surprising that its scaling exponents are very similar to those observed in velocity. This is true in the case of subAlfvénic models, because all curves in the middle left plot in Figure 6 are tightly covering the S-L scaling with $D = 1$. The similarity between the velocity and its solenoidal part is also confirmed in the case of superAlfvénic models but only for subsonic case, when the role of shocks is strongly diminished. Two supersonic models show exponents following a scaling more closer to the S-L one with $D = 1$, yet still with lower values for $p > 3$. The scal-

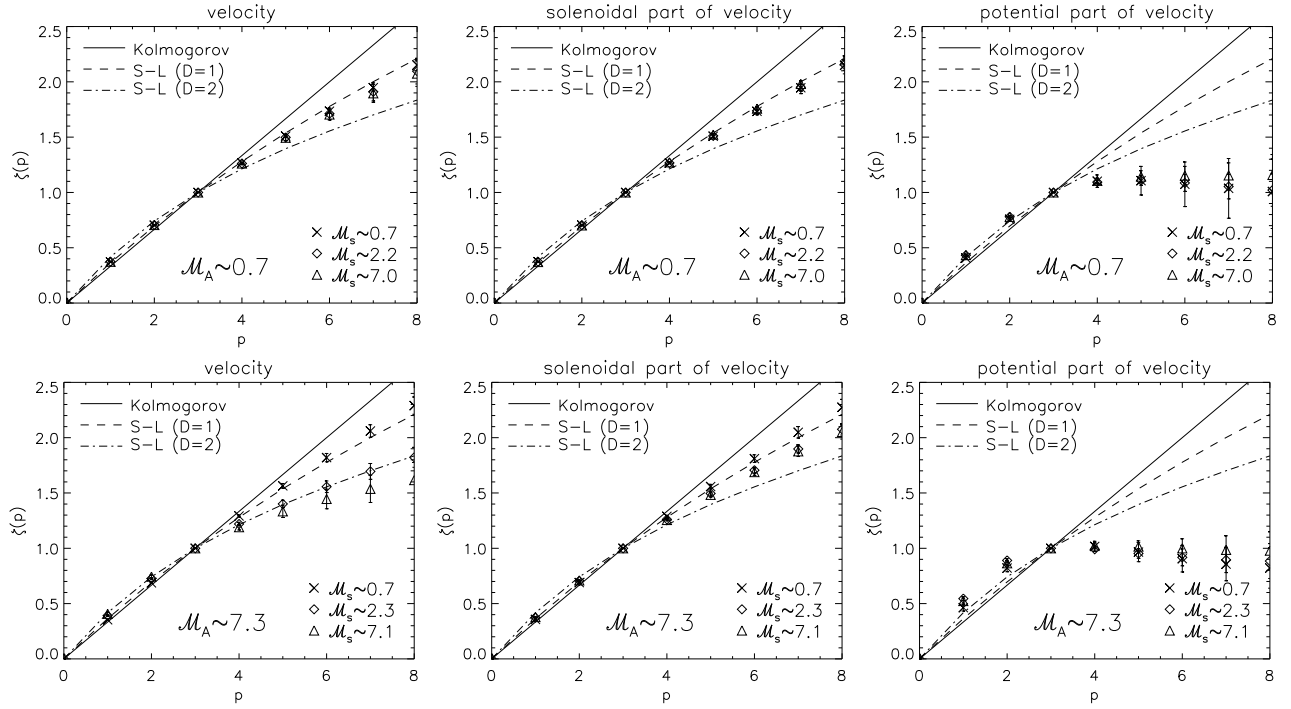


FIG. 6.— Scaling exponents of the velocity (left column) and its incompressible and compressible parts (middle and right columns, respectively) for experiments with different sonic Mach numbers in two regimes: subAlfvénic (upper row) and superAlfvénic (lower row).

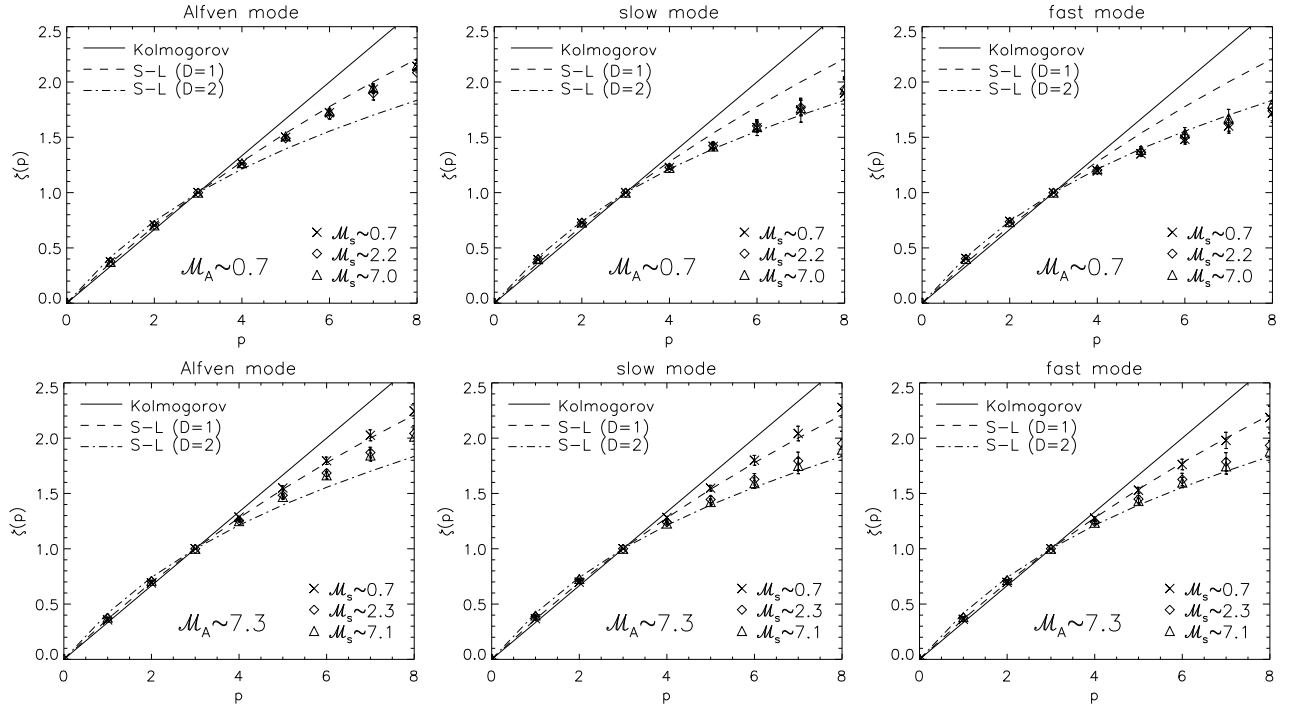


FIG. 7.— Scaling exponents of the Alfvén, slow and fast modes of the velocity (left, middle and right columns, respectively) for experiments with different sonic Mach numbers in two regimes: subAlfvénic (upper row) and superAlfvénic (lower row).

ings of structure of the compressible part, shown in the right column of Figure 6, cannot be compared to any of the theoretical models. Their scalings signify dissipative structures with dimensions higher than two, but the theory may be not applicable here. In order to explain what these scaling exponents represent we should describe what could be a physical picture of the compressible part of the velocity field. First of all, the compressible part is much weaker than the incompressible one, thus the structure functions of higher orders amplify rare events in the structure, such as individual regions compressed by shocks. This is supported by the huge error bars increasing with the value of p signifying that these rare events may have poor statistics or can change rapidly contributing differently at different times and in different models. In such situations the scaling exponents for higher values of p are not reliable.

Another decomposition, which separate velocity into the MHD waves, gives an opportunity to calculate their scaling relations as well. In Figure 7 we present the scaling exponents for the Alfvén, slow and fast waves. The Alfvén wave is presented in plots in the left column. Comparing these plots with the corresponding plots for the solenoidal part of the velocity reveals obvious conclusion that the Alfvén wave due to its incompressibility should follow exactly the same scaling as the incompressible part. This is visible in these two plots clearly. Scaling exponents of the solenoidal part and the Alfvén mode match nicely in plots for subAlfvénic models with a weaker dependency of the sonic Mach number and for superAlfvénic models where the dependency of \mathcal{M}_s is stronger. Two other modes, the slow and fast waves presented in the middle and right columns of Figure 7, respectively, show similar scaling relations. For example, the scaling exponents for slow and fast waves in the subAlfvénic turbulence follow the S-L scaling with $D = 2$ and depend on the sonic Mach number marginally. This signifies that the two-dimensional structures dominate in both components. For superAlfvénic turbulence the scalings of these two waves show a somewhat different situation. Both components, the slow and fast waves, have similar values of scaling exponents ζ , but they change with the sonic Mach number. We see that for subsonic turbulence most of dissipative structures of the slow and fast waves is one-dimensional. Scaling exponents follow very precisely the S-L scaling with $D = 1$. In the case of supersonic turbulence, however, these scalings suggest the two-dimensional dissipative structures again, similarly to the subAlfvénic turbulence. This signifies an important role of the magnetic field in the generation of the structures of different dimensions in the subsonic turbulence.

The above considerations were carried for the scalings relations in the global reference frame, i.e., when we do not take the direction of the local magnetic field into account. The strong magnetic field is dynamically important in subAlfvénic turbulence and can greatly influence the generation of the structure, thus the statistical methods which include also its local direction in the analysis can give a substantial insight into the physics of turbulence with the presence of the magnetic field. In Figure 8 we show scaling exponents calculated in the local reference frame for velocity and its incompressible and compressible parts. Starting from the subAlfvénic turbulence, which are shown on two upper rows (for parallel and perpendicular directions, respectively), we see that the scaling exponents are different depending on the direction. For example, the structures of velocity in the direction perpendicular to the local field are one-dimensional, as suggested by the plot in the second row on the left in Figure 8. This scal-

ings are very similar to those calculated in the global reference frame. However, the same velocity field in the direction along the local magnetic field have different structures with higher dimensions than two, according to the corresponding plots. Both scalings, in parallel and perpendicular directions, depend on the sonic Mach number only marginally. Next, the solenoidal component shown in the middle column of figure 8 have a similar property. Its structures in the perpendicular direction are very similar to that observed in the global reference frame while in the parallel direction its structures are two-dimensional. Again, the potential component, although its scaling relation cannot be explained by the current theoretical models, have scaling relations in the perpendicular direction very similar to that in the global reference frame. All these observations signify that the dominant structures are created in the directions perpendicular to the local field, while the parallel structures are less significant and usually have more dimensions. We see that in these models the role of the magnetic field in generation of the structure is very clear. What do we expect when the magnetic field is weaker in such turbulence.

Now, we compare the scaling exponents of MHD waves obtained in the local reference frame which are presented in Figure 9. The Alfvén wave which is incompressible and directed perpendicularly to the local magnetic field is presented in the left column of Figure 9. In the subAlfvénic turbulence when the magnetic field is strong we expect that the most of the structure of the Alfvén mode should be generated in the direction perpendicular to the local magnetic field. This is confirmed by the corresponding plots in Figure 9. The scaling exponents in the perpendicular direction are consistent with those in the global reference frame (Figure 7). The scalings suggest the one-dimensional dissipative structures in all subAlfvénic models independently of the sonic Mach number. In the parallel direction the plot suggests the dissipative structures with higher direction but at the same time we see very large error bars which signify very poor statistics. It means that the structures of the Alfvén wave created in the direction parallel to the local field are marginal. On the contrary, the slow wave has direction parallel to the local mean magnetic field, what signifies that its dissipative structure should be more dominant in the parallel direction. Indeed, the slow wave in the parallel direction has structures consistent with those observed in the global mean magnetic field while in the perpendicular direction it shows some random, rare events in the structure.

7. DISCUSSION

7.1. Major Accomplishments and Limitations of the Present Study

In the paper we have introduced a new procedure of decomposition of MHD turbulence field into Alfvén, slow and fast modes which uses wavelets. Compared to the decomposition procedure based on Fourier transforms described in CL03, the wavelet decomposition is more local, thus it follows better the local magnetic field direction in respect to which the decomposition into modes takes place. As a result, we expect that the wavelet decomposition procedure to be more accurate for larger amplitudes of turbulence, i.e. larger perturbations of magnetic field.

Our decomposition of the MHD turbulence confirmed the results in CL03 in terms of spectra, namely, that the Alfvénic and slow modes are anisotropic and consistent with

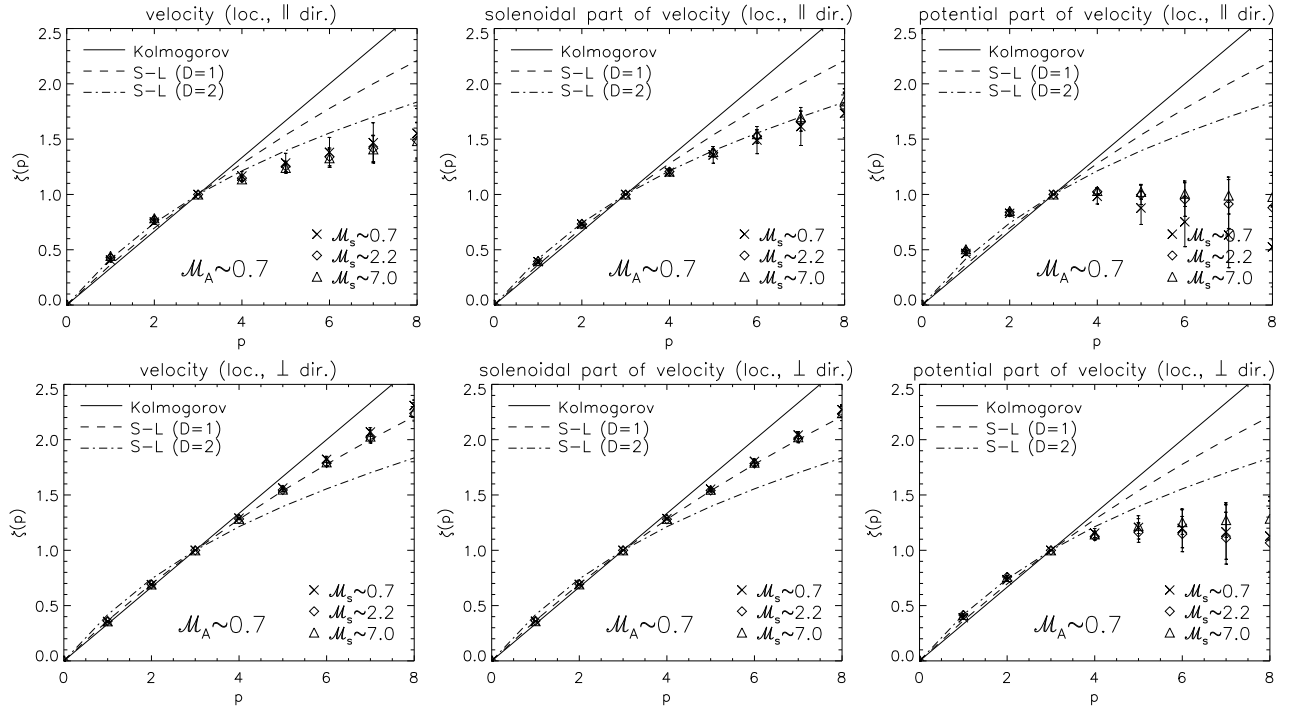


FIG. 8.— Scaling exponents of the velocity and its solenoidal and potential parts (left, middle and right columns, respectively) calculated in the local reference frame. Two rows show the scalings exponent at the parallel and perpendicular direction the local mean magnetic field for models with a strong magnetic field.

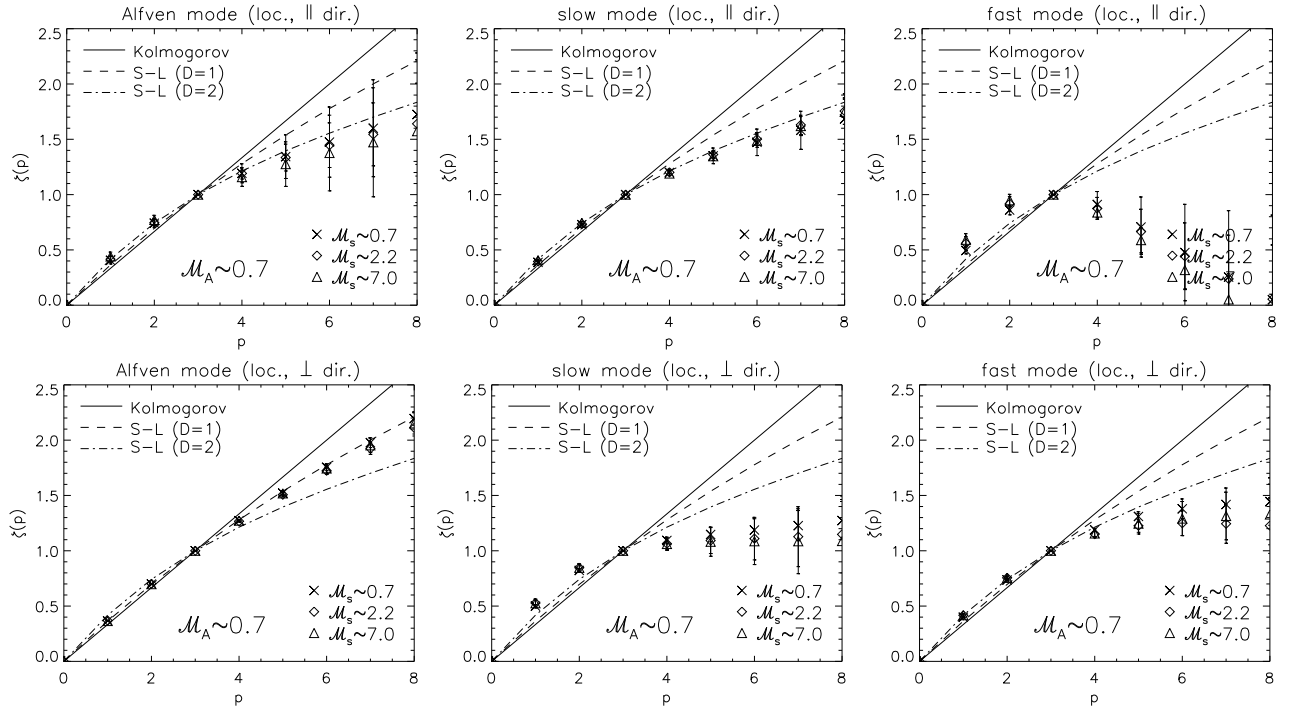


FIG. 9.— Scaling exponents of the Alfvén, slow and fast waves of the velocity (left, middle and right columns, respectively) calculated in the local reference frame. Two rows show the scalings exponent at the parallel and perpendicular direction the local mean magnetic field for models with a strong magnetic field.

the predictions of the GL95 model of incompressible turbulence, while the fast modes are mostly isotropic and form an acoustic turbulence cascade (Lithwick & Goldreich 2001; Cho & Lazarian 2002). As these results were used in studies of cosmic ray scattering and acceleration (Yan & Lazarian 2002, 2004, 2008; Cho & Lazarian 2005; Brunetti & Lazarian 2007) as well as charged dust acceleration (Lazarian & Yan 2002; Yan & Lazarian 2003; Yan et al. 2004; Yan 2009) this is an encouraging development.

At the same time, the intermittency of the different MHD modes were shown to be very different. We clearly see the dependence of high order statistics of compressible motions on the Mach number. We interpret this dependence as the result of shock formation, which eventually changes the nature of the compressible motion cascade compared to the CL03 assumptions.

The limitations of the present study arise from the yet unclear nature of the turbulent cascade. For instance, it was shown in Beresnyak & Lazarian (2009) that the degree of locality of interactions in hydrodynamic and MHD cascade are different. Thus even largest available MHD simulations may not present the actual inertial range of the cascade, but the measured slope may be strongly affected by the extended bottle-neck effect of the simulations. In addition, the limited range over which Alfvénic turbulence is weak may exhibit a rather different scaling of fast modes as a result of the interactions of the Alfvénic and fast modes (Chandran 2005).

In addition, within the present study we intentionally do not consider the scaling of magnetic perturbations. The velocity and magnetic perturbations for subAlfvénic turbulence show some differences, which are rather difficult to study reliably with the available numerical simulations. These differences are not a part of the GS95 picture, but may reflect additional yet unclear properties of the MHD cascade (see Müller & Biskamp 2000).

In our study we used only the incompressible driving. In the presence of the compressible supersonic driving (Federrath et al. 2009) the scaling looks different, but the existence of the inertial range is then questionable. Kritsuk et al. (2009) claimed that combining the compressible and incompressible driving in the Mach number dependent fashion one can obtain a better power-law inertial range. This issue requires further studies.

The turbulence driving in our study is balanced, in the sense that the energy flows in opposite directions are equal. In the presence of sources and sinks of turbulent energy, astrophysical turbulence is expected to be imbalanced. Our numerical studies of imbalanced turbulence in Beresnyak & Lazarian (2010) show that the properties of Alfvénic turbulence changes substantially in the presence of imbalance. However, the degree of sustainable imbalance in compressible turbulence is still unclear. One expects the density fluctuation in turbulent fluid to reflect the incoming waves, altering the imbalance. We believe that in high Mach number fluids the imbalance is low due to the existence of substantial density contrasts.

7.2. Astrophysical Implications of the Turbulence Anisotropy and Intermittency

Depending on driving astrophysical turbulence may be sub-Alfvénic, if the injection velocity V_L is less than Alfvén speed V_A , Alfvénic, if $V_L = V_A$, and superAlfvénic, if $V_L > V_A$. This frequently is also described by the Alfvén Mach number $M_A = V_L/V_A$. Formally, the GS95 model applies only to incompressible

motions with $V_L = V_A$, or equivalently $M_A = 1$. Some of the astrophysical applications of the model, indeed, use the original form of the theory, which substantially limits the applications of the theory (see Narayan & Medvedev 2001). However, the model can be easily generalized to cover extensive ranges of superAlfvénic and subAlfvénic turbulence (see Lazarian & Vishniac 1999; Lazarian 2006). For subAlfvénic turbulence with isotropic driving at the scale L an initial weak cascade, in which the parallel scale of motions stays the same and the spectrum $E(k_\parallel) \sim k_\parallel^{-2}$ is applicable, transfers to the regime of strong turbulence at the scale of LM_A^2 , for which the GS95 critical balance arguments are applicable. For superAlfvénic turbulence, while up to the scale LM_A^{-3} the turbulence is hydrodynamic, it approaches the GS95-type regime for smaller scales. Therefore, the relations obtained for MHD turbulence that we have studied above can be generalized for cases of different intensity of driving.

While the GS95 model is a model of incompressible turbulence, our simulations confirm the numerical findings in Cho & Lazarian (2002) and CL03 that the scaling of the Alfvénic mode in the compressible turbulence is very similar to its scaling in the incompressible case. In particular, the GS95 anisotropy of MHD turbulence determines the rate of magnetic field wandering which is important for many astrophysical processes, including the ubiquitous process of magnetic reconnection (Lazarian & Vishniac 1999). Additional implications of magnetic field wandering include the diffusion of heat and cosmic rays, MHD acceleration of dust etc. (see Lazarian et al. 2009, for a review). The wavelet approach has the potential of increasing accuracy while studying small-scale anisotropy in simulations with strongly perturbed magnetic fields.

Falgarone et al. (2005, 2006, 2007) and collaborators (Hily-Blant & Falgarone 2007; Hily-Blant et al. 2007, and refs. therein) attracted the attention of the interstellar community to the potential important implications of intermittency. A small and transient volume with high temperatures or violent turbulence can have significant effects on the net rates of processes within the ISM. For instance, many interstellar chemical reactions (e.g., the strongly endothermic formation of CH^+) might take place within very intensive intermittent vortices. The aforementioned authors claimed the existence of the observational evidence for such reactions and heating, but a more quantitative approach to the problem is possible. Beresnyak & Lazarian (2007) (see also Lazarian et al. 2009) used the intermittency scaling and calculated the distribution of the dissipation rate in the turbulent volumes. In doing so they used the fact that She & Lévéque (1994) model of intermittency corresponds generalized log-Poisson distribution of the local dissipation rates Dubrulle (1994); She & Waymire (1995). The obtained rates of enhancement were not sufficient to explain the heating required for inducing interstellar chemistry (Beresnyak & Lazarian 2007). The same approach was used by Pan et al. (2009) who obtained, however, a different result. We believe that one should distinguish shocks from vortical motions while calculating the heating induced by intermittency. Our present study show very different scalings relevant to these types of motions.

7.3. Studies of Compressible MHD Turbulence in Astrophysical Context

Numerous studies of compressible MHD turbulence are done in the context of star formation (see reviews by

Mac Low et al. & Klessen 2004; McKee & Ostriker 2007, and references therein). Most of these simulations are focused on the large-scale appearances of the turbulence, which is determined by the turbulent driving and do not exhibit any extended inertial range of turbulence.

Search for the universal relations for compressible turbulence resulted in the rise of interest to the Fleck (1983) idea of searching universality not for velocity, but for the combination of the velocity and density in the form $\rho^{1/3}v$. The numerical study of hydrodynamic compressible turbulence revealed that, indeed, the density modified velocity shows the same Kolmogorov scaling both for low and high Mach number turbulence (Kritsuk et al. 2007). Similar effect was confirmed in our MHD simulations Kowal & Lazarian (2007). However, the physical justification of this universality is unclear and it may result just from the coincidental compensation of the change of velocity and density indexes as shocks develop at high Mach number turbulence.

We report steepening of the spectra of compressible motions at high Mach numbers. High resolution hydro simulations (see Kritsuk et al. 2007) show that the velocity spectrum becomes steeper for high Mach number simulations. This corresponds to the observational studies of the supersonic velocity turbulence in Padoan et al. (2006, 2009) and Chepurnov et al. (2006). These studies are done with the Velocity Channel Analysis (VCA) and Velocity Coordinate Spectrum (VCS) techniques, which are theory-motivated and tested techniques (Lazarian & Pogosyan 2000, 2004, 2006, 2008; Chepurnov et al. 2008). The application of these techniques should enhance the range of astrophysical turbulent velocity fields that can be studied observationally² It is comparing numerics, observations and theory that the progress in understanding of turbulence requires.

8. SUMMARY

In this article we presented a new technique of decomposition of turbulent MHD motions into Alfvén, slow and fast modes. The technique is based on the use of wavelets, which provide a more local decomposition compared to the Fourier approach in CL02 and CL03. This enables one to have better accuracy of the decomposition of MHD turbulence into fundamental modes for higher amplitude of magnetic perturbations.

By applying the wavelet decomposition to the results of our simulations of compressible MHD turbulence, we investigated the scaling properties of velocity in compressible MHD

turbulence for different sonic M_s and Alfvénic M_A Mach numbers. We analyzed spectra, the anisotropy, scaling exponents and intermittency of the total velocity and its components corresponding to the Alfvén, slow and fast modes. We found that:

- The amplitude of velocity fluctuations depends on M_s only marginally. The lack of significant dependence of the velocity fluctuations is also observed for its incompressible part, as well as for the Alfvén and slow waves. The compressible part of velocity and the fast wave show a dependence on M_s , but only for subsonic turbulence. In the case of supersonic models, the fluctuations of the compressible part and fast mode of the velocity have comparable amplitudes.
- The spectral indices depend on M_A in turbulence with a strong magnetic field. In the case of turbulence with a weak magnetic field only the indices of spectra of the fast wave change between sub- and supersonic models. For the other components, the spectral indices do not change appreciably with the sonic Mach number. While our conclusions about spectra of fast modes for subsonic turbulence agree with the CL03 conclusion about the acoustic cascade of these modes, we feel that for high Mach number we get the spectrum of shocks. The anisotropy of Alfvénic turbulence and slow modes is in agreement with GS95 theory for both the cases of high and low beta plasmas. The velocity fluctuations of the fast modes demonstrate isotropy.
- In the global reference frame, we observe stronger changes of the scaling exponents and intermittency for velocity and its all components with M_s in the case of turbulence with a weak magnetic field. The intermittency of structures grows with the values of M_s . However, when the external magnetic field is strong, the intermittency for all components depends on the sonic Mach number only marginally. In the local reference frame, the scaling exponents turbulence depend on the direction with respect to the direction of the local mean magnetic field. The dependence is stronger for the sub-Alfvénic turbulence.

Our research is supported by the NSF grant AST-0808118 and the Center for Magnetic Self-Organization in Astrophysical and Laboratory Plasmas.

REFERENCES

- Antoine, J.-P. 1999, *Wavelets in Physics*, Edited by J. C. van den Berg, Published by Cambridge University Press
- Beresnyak, A., Lazarian, A. & Cho, J., 2005, ApJ, 624, L93
- Beresnyak, A., & Lazarian, A. 2007, KITP talk, <http://online.itp.ucsb.edu/online/stars07/lazarian/>
- Beresnyak, A. & Lazarian, A. 2009, ApJ, 702, 1190
- Beresnyak, A. & Lazarian, A. 2010, in press, (arXiv:1002.2428)
- Biskamp, D. 2003, *Magnetohydrodynamic Turbulence*, Cambridge, UK: Cambridge University Press
- Brunetti, G., & Lazarian, A. 2007, MNRAS, 378, 245
- Burkhart, B., Falceta-Gonçalves, D., Kowal, G., & Lazarian, A. 2009, ApJ, 693, 250
- Burkhart, B., Stanimirović, S., Lazarian, A., & Kowal, G. 2010, ApJ, 708, 1204
- Chandran, B. D. G. 2005, Physical Review Letters, 95, 26, 5004
- Cho, J. & Vishniac, E. T., 2000, ApJ, 539, 273
- Cho, J. & Lazarian, A., 2002, Phys. Rev. Lett., 88, 245001
- Cho, J., Lazarian, A. & Vishniac, E. T. 2002, ApJ, 564, 291
- Cho, J. & Lazarian, A., 2003, MNRAS, 345, 325, CL03
- Cho, J., Lazarian, A., & Vishniac, E. T. 2003, ApJ, 595, 812
- Cho, J., & Lazarian, A. 2005, Theoretical and Computational Fluid Dynamics, 19, 127
- Dobrowolny, M., Mangeney, A., & Veltri, P. 1980, Physical Review Letters, 45, 144
- Dubrulle, B. 1994, Phys. Rev. Lett., 73, 959
- Elmegreen, B. G., & Scalo, J. 2004, ARA&A, 42, 211
- Falgarone, E., Hily-Blant, P., Pety, J., & Pineau Des Forêts, G. 2005, proceedings of the conference *Magnetic Fields in the Universe: From Laboratory and Stars to Primordial Structures.*, American Institute of Physics Conference Series, 784, 299, edited by E. M. de Gouveia dal Pino, G. Lugones, & A. Lazarian
- Falgarone, E., Pineau Des Forêts, G., Hily-Blant, P., & Schilke, P. 2006, A&A, 452, 511
- Chepurnov, A. et al., 2006, in press, (arXiv:astro-ph/0611462)
- Chepurnov, A. et al., 2008, ApJ, 688, 1021

² Recent examples of the techniques of observational studies of the turbulent density field can be found in Kowal et al. (2007); Burkhart et al. (2009, 2010). The velocity is a more covered statistics, but it is more difficult to study (see Lazarian 2009, for a review).

- Falgarone, E., Levrier, F., & Hily-Blant, P. 2007, EAS Publications Series, 23, 73
- Federrath, C., Klessen, R. S., & Schmidt, W. 2008, ApJ, 688, L79
- Federrath, C., Klessen, R. S., & Schmidt, W. 2009, ApJ, 692, 364
- Fleck, R. C. Jr., 1983, ApJ, 272, L45
- Goldreich, P., Sidhar, S., 1995, ApJ, 438, 763, GS95
- Galtier, S., Nazarenko, S. V., Newell, A. C., & Pouquet, A. 2000, Journal of Plasma Physics, 63, 447
- Higdon, J. C. 1984, ApJ, 285, 109
- Hily-Blant, P., & Falgarone, E. 2007, A&A, 469, 173
- Hily-Blant, P., Pety, J., & Falgarone, E. 2007, proceedings of the "SINS - Small Ionized and Neutral Structures in the Diffuse Interstellar Medium", Astronomical Society of the Pacific Conference Series, edited by M. Haverkorn & W. M. Goss, 365, 184
- Kowal, G., Lazarian, A., & Beresnyak, A. 2007, ApJ, 658, 423
- Kowal, G. & Lazarian, A., 2007, ApJ, 666, L69
- Kowal, G., Lazarian, A., Vishniac, E. T., & Otmianowska-Mazur, K. 2009, ApJ, 700, 63
- Kritsuk, A. G., Norman, M. L., Padoan, P., & Wagner, R. 2007, ApJ, 665, 416
- Kritsuk, A. G., Ustyugov, S. D., Norman, M. L., & Padoan, P. 2009, 180, 1, 2020
- Lazarian, A., & Vishniac, E. T. 1999, ApJ, 517, 700
- Lazarian, A. & Pogosyan, D., 2000, ApJ, 537, 720
- Lazarian, A. & Yan, H. 2002, ApJ, 566, L105
- Lazarian, A. & Pogosyan, D., 2004, ApJ, 616, 943
- Lazarian, A. 2006, ApJ, 645, L25
- Lazarian, A. & Pogosyan, D., 2006, ApJ, 652, 1348
- Lazarian, A. & Pogosyan, D., 2008, ApJ, 686, 350
- Lazarian, A. 2009, Space Science Reviews, 143, 357
- Lazarian, A., Beresnyak, A., Yan, H., Opher, M., & Liu, Y. 2009, Space Science Reviews, 143, 387
- Levy, D., Puppo, G. & Russo, G. 1999, Mathematical Modelling and Numerical Analysis, 33, 547
- Lithwick, Y. & Goldreich, P. 2001, ApJ, 562, 279
- Liu, X.-D. & Osher, S. 1998, Journal of Computational Physics, 142, 304
- MacLow, M.-M. 2004, Ap&SS, 289, 323
- Mac Low, M.-M. & Klessen, R. S., 2004, Reviews of Modern Physics, 76, 125
- Maron, J. & Goldreich, P. 2001, ApJ, 554, 1175
- Matthaeus, W. H., Montgomery, D. C., & Goldstein, M. L. 1983, Physical Review Letters, 51, 1484
- McKee, C. F., & Ostriker, E. C. 2007, ARA&A, 45, 565
- Meneveau, C. 1991, Physical Review Letters, 66, 1450
- Meneveau, C. 1991, Journal of Fluid Mechanics, 232, 469
- Montgomery, D. & Turner, L. 1981, Physics of Fluids, 24, 825
- Müller, W. C. & Biskamp, D., 2000, Phys. Rev. Lett., 84, 3
- Narayan, R., & Medvedev, M. V. 2001, ApJ, 562, L129
- Novikov, E. A., 1994, Phys. Rev. E, 50, 3303
- Oughton, S., Dmitruk, P., & Matthaeus, W. H. 2003, Lecture Notes in Physics, 614, 28
- Padoan, P., Juvela, M., Kritsuk, A., & Norman, M. L. 2006, ApJ, 653, L125
- Padoan, P., Juvela, M., Kritsuk, A., & Norman, M. L. 2009, ApJ, 707, L153
- Pan, L., Padoan, P., & Kritsuk, A. G. 2009, Phys. Rev. Lett., 102, 034501
- She, Z. & Lévéque, E., 1994, Phys. Rev. Lett., 72, 3
- She, Z.-S. & Waymire, E. C., 1995, Phys. Rev. Lett., 74, 262
- Shebalin, J. V., Matthaeus, W. H., & Montgomery, D. 1983, Journal of Plasma Physics, 29, 525
- Tóth, G. 2000, Journal of Computational Physics, 161, 605
- Yan, H. & Lazarian, A. 2002, Physical Review Letters, 89, B1102
- Yan, H., & Lazarian, A. 2003, ApJ, 592, L33
- Yan, H., & Lazarian, A. 2004, ApJ, 614, 757
- Yan, H., Lazarian, A., & Draine, B. T. 2004, ApJ, 616, 895
- Yan, H., & Lazarian, A. 2008, ApJ, 673, 942
- Yan, H. 2009, MNRAS, 397, 1093